iScience

CellPress
OPEN ACCESS

Article

The role of long noncoding RNA Nron in atherosclerosis development and plaque stability

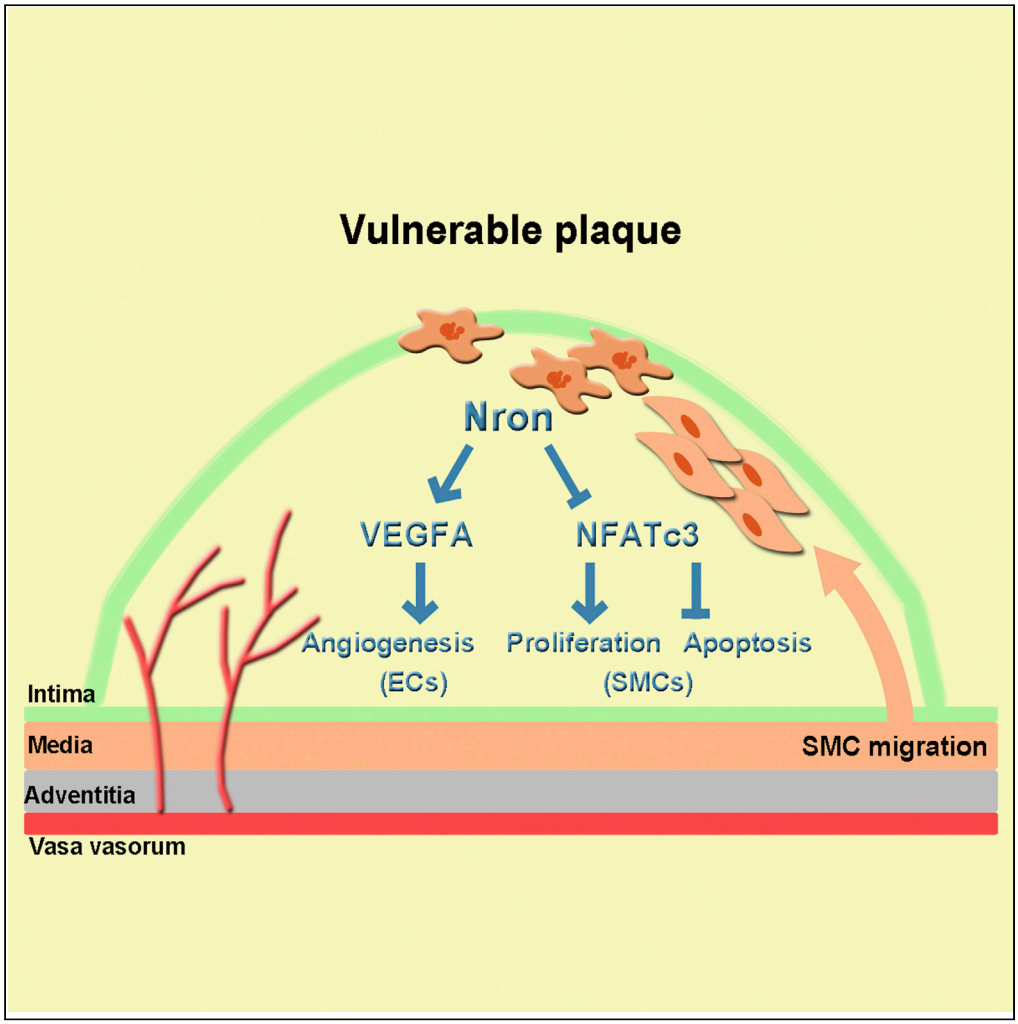

Meng Du, Cheng Wang, Liuye Yang, ..., Jiangtong Peng, Dan Huang, Kai Huang

d201378184@alumni.hust.edu.cn (M.D.)
unionhuang@163.com (K.H.)

Highlights

Nron promotes atherosclerosis progression and contributes to plaque instability

Nron negatively regulates NFATc3 activity and impairs VSMC function

Nron increases VEGFA production and promotes intra-plaque angiogenesis

Du et al., iScience 25, 103978
March 18, 2022
https://doi.org/10.1016/j.isci.2022.103978

iScience

CellPress
OPEN ACCESS

Article

The role of long noncoding RNA Nron in atherosclerosis development and plaque stability

Meng Du,[1,2,3,4,5,*] Cheng Wang,[1,2,4] Liuye Yang,[1,2] Bing Liu,[1,2] Zhe Zheng,[1,2] Liu Yang,[1,2] Fengxiao Zhang,[1,2] Jiangtong Peng,[1,2] Dan Huang,[1,2] and Kai Huang[1,2,3,*]

SUMMARY

The major clinical consequences of atherosclerosis such as myocardial infarction or stroke are because of thrombotic events associated with acute rupture or erosion of an unstable plaque. Here, we identify an lncRNA Noncoding Repressor of NFAT (Nron) as a critical regulator of atherosclerotic plaque stability. Nron overexpression (OE) in vascular smooth muscle cells (VSMC) induces a highly characteristic architecture of more-vulnerable plaques, while Nron knockdown (KD) suppresses the development of atherosclerosis and favors plaque stability. Mechanistically, Nron specifically binds to and negatively regulates NFATc3, thus inhibiting the proliferation and promoting the apoptosis of VSMCs. Moreover, we also provide evidence that Nron increases the production and secretion of VEGFA from VSMCs, which functions as a paracrine factor to enhance intra-plaque angiogenesis. All of these effects contribute to plaque instability. Genetic or pharmacological inhibition of Nron may have potential for future therapy of atherosclerosis.

INTRODUCTION

Atherosclerosis is a systemic disease characterized by interactions among multiple kinds of cells which result in local inflammation of the arterial wall (Glass and Witztum, 2001; Lusis, 2000). Despite substantial improvements in our understanding of mechanisms contributing to atherosclerosis and overall reduction in cardiovascular mortality, the absolute disease burden remains substantially high. The major clinical consequences of atherosclerosis such as myocardial infarction or stroke are not a function of gradual narrowing of the lumen, but rather because of thrombotic events associated with acute rupture or erosion of an unstable plaque. Vascular smooth muscle cells (VSMCs) play a pivotal role in atherogenesis and have historically been considered beneficial for plaque stability, because they constitute the main cellular component of the protective fibrous cap within lesions and are responsible for synthesizing strength-giving extracellular matrix components (Allahverdian et al., 2018). Accordingly, loss of VSMCs or their function in advanced plaques has detrimental effects, leading to fibrous cap thinning, necrotic core formation, and plaque erosion (Grootaert et al., 2018).

Long noncoding RNAs (lncRNAs) are a group of nonprotein-coding RNAs that are greater than 200 nucleotides in length. Although a bulk of studies have focused on the contribution of lncRNAs in cellular development and differentiation, rapidly accumulating evidence suggests an additional contribution of lncRNAs in cardiovascular disease such as atherosclerosis (Zhang et al., 2018). Recently, more and more lncRNAs interfering with the progress of atherosclerosis were identified and characterized in the atherogenic cells such as VSMCs, endothelial cells (ECs), and monocytes/macrophages (Holdt et al., 2019; Kraczkowska and Jagodzinski, 2019; Yan et al., 2020). Modulation of lncRNA may potentially offer promising diagnostic and therapeutic strategies to reduce atherosclerosis burden.

The lncRNA noncoding repressor of NFAT (Nron) is about 2.7 kb in length and is composed of three exons, which can be alternatively spliced to yield transcripts ranging in size from 0.8 to 3.7 kb (Imam et al., 2015). It was reported to contribute to the assembly of a large RNA/protein complex and function as a cytoplasmic trap for phosphorylated Nuclear Factor of Activated T cells (NFAT) proteins in T lymphocytes (Sharma et al., 2011; Willingham et al., 2005). Although originally thought to be restricted to immune system and to play an

[1]Department of Cardiology, Union Hospital, Tongji Medical College, Huazhong University of Science and Technology, 1277 Jiefang Ave., Wuhan 430000 China

[2]Clinic Center of Human Gene Research, Union Hospital, Tongji Medical College, Huazhong University of Science and Technology, Wuhan, China

[3]Liyuan Cardiovascular Center, Tongji Medical College, Huazhong University of Science and Technology, Wuhan, China

[4]These authors contributed equally

[5]Lead contact

*Correspondence: d201378184@alumni.hust.edu.cn (M.D.), unionhuang@163.com (K.H.)

https://doi.org/10.1016/j.isci.2022.103978

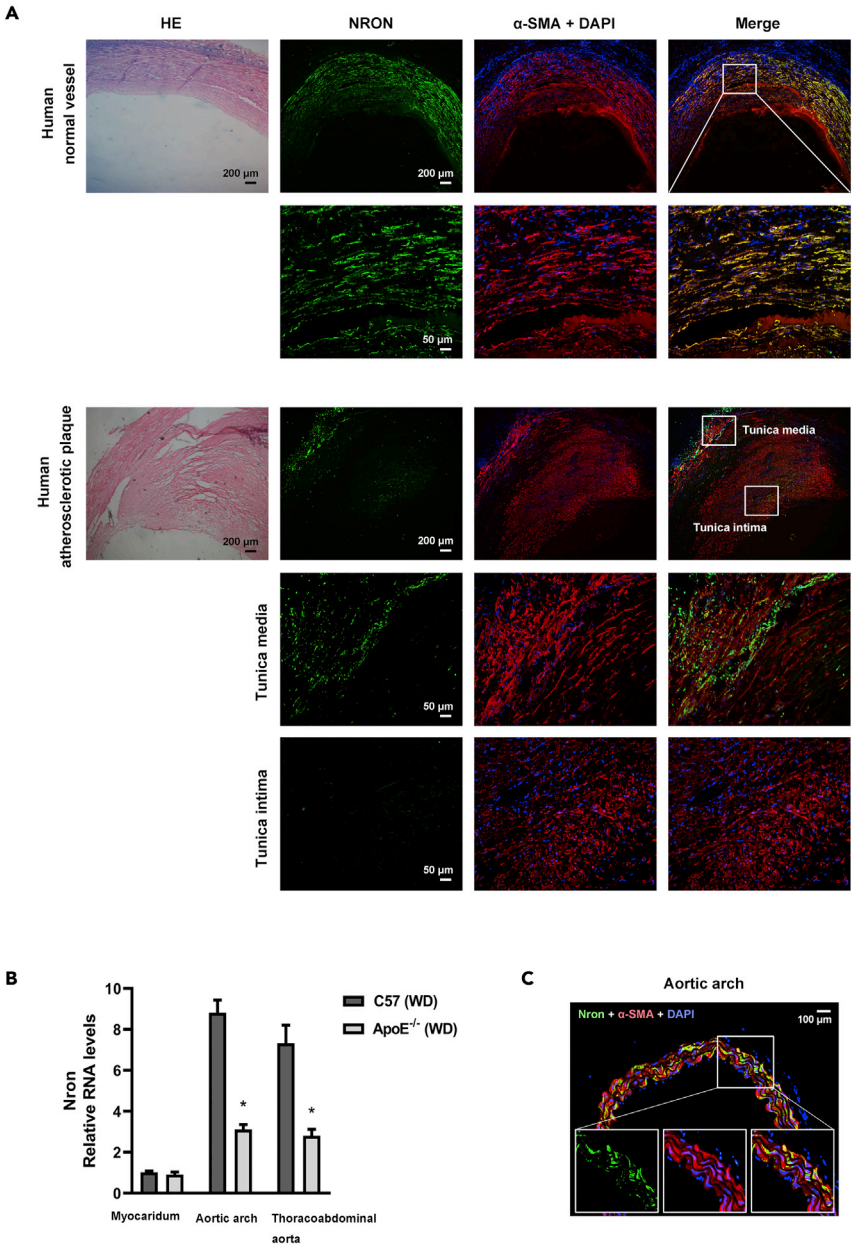

Figure 1. The expression of Nron is downregulated in atherosclerotic lesions from human and mice

(A) RNA FISH analysis of NRON in human normal vessels (*upper panel*) and carotid atherosclerotic lesions (*lower panel*). For colocalization analysis, sections were co-stained for NRON (green) and α-SMA (red; smooth muscle cell marker). 4′,6-diamidino-2-phenylindole (DAPI) was used for nucleus staining (blue).

(B) 6-week male ApoE$^{-/-}$ or wild type mice were fed a western diet (WD) for 12 weeks. Relative expression of Nron in the aortic arch, thoracoabdominal aorta, and myocardium were determined.

(C) RNA FISH analysis of Nron in the aortic arch from wild type mice. For colocalization analysis, sections were co-stained for Nron (green) and α-SMA (red; smooth muscle cell marker). DAPI was used for nucleus staining (blue).

important role in the differentiation of T cells, Nron has since been shown to regulate different pathophysiological processes and involve in many other diseases (Li et al., 2016; Liu et al., 2011; Niu et al., 2019). In the present work, we explore the involvement of Nron in the progression of atherosclerosis, and reveal a previously-unsuspected role of Nron in smooth muscle function and intra-plaque angiogenesis which are implicated in the regulation of plaque stability.

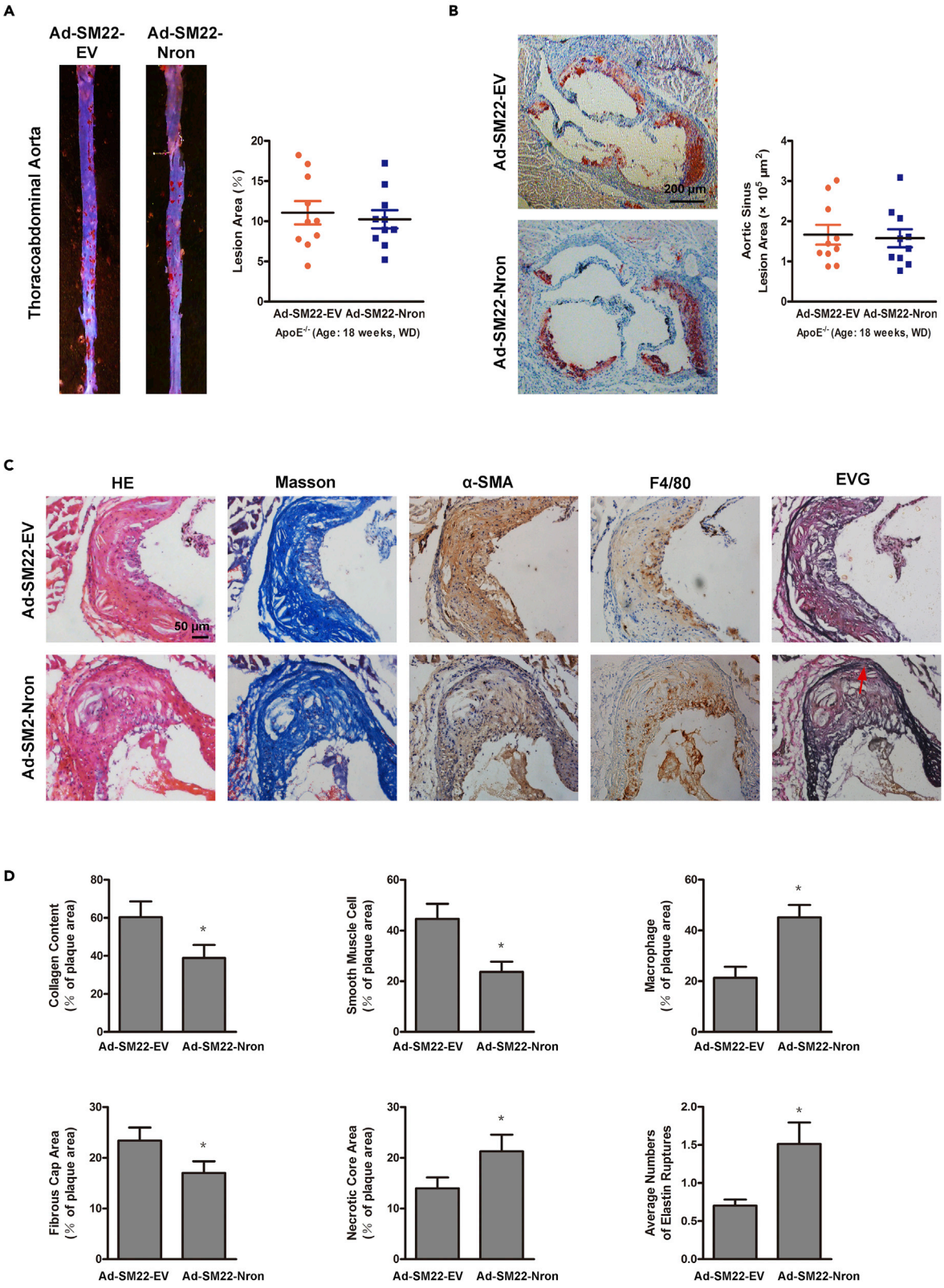
A
Ad-SM22-EV
Ad-SM22-Nron
Thoracoabdominal Aorta
Lesion Area (%)
Ad-SM22-EV Ad-SM22-Nron
ApoE-/- (Age: 18 weeks, WD)
B
Ad-SM22-EV
Ad-SM22-Nron
200 μm
Aortic Sinus Lesion Area (× 10^5 μm^2)
Ad-SM22-EV Ad-SM22-Nron
ApoE-/- (Age: 18 weeks, WD)
C
HE
Masson
α-SMA
F4/80
EVG
Ad-SM22-EV
Ad-SM2-Nron
50 μm
D
Collagen Content (% of plaque area)
Smooth Muscle Cell (% of plaque area)
Macrophage (% of plaque area)
Fibrous Cap Area (% of plaque area)
Necrotic Core Area (% of plaque area)
Average Numbers of Elastin Ruptures
Ad-SM22-EV Ad-SM22-Nron

Figure 2. Nron overexpression induces a highly characteristic architecture of more-vulnerable plaques

6-Week male ApoE$^{-/-}$ mice were fed a western diet for 16 weeks. Mice were intravenously administered with adenovirus (Ad-SM22-EV or Ad-SM22-Nron) every two weeks in the last 8 weeks before being sacrificed.

(A) Oil Red O staining of thoracoabdominal aorta, and lipid accumulation was quantified as percentage of total surface area of aorta.

(B) Images and quantification of Oil Red O staining in lesions of aortic sinus.

(C) Representative images of aortic sinus for H&E (HE), Masson's trichrome (Masson), Elastica van Gieson (EVG), smooth muscle cells (α-SMA), and macrophages (F4/80). Arrows in EVG staining panels indicate ruptures of elastic fibers of tunica media.

(D) Quantification of collagen content, fibrous cap area, necrotic core area, ruptures of elastic fibers, macrophage content, and smooth muscle cell content. Data are expressed as mean ± SEM (n = 12 per group). Statistical analysis was performed using Student's t test. *p <0.05 vs. Ad-SM22-EV group.

RESULTS

The expression of Nron is downregulated in atherosclerotic lesions from human and mice

To clarify the role of Nron in atherogenesis, we firstly examined its expression in human carotid atherosclerotic plaques and internal mammary arteries (normal vessels). Fluorescence *in situ* hybridization (FISH) combined with immunostaining showed that Nron was expressed in abundance in healthy vessels and co-localized predominantly with α-SMA^{+} SMCs; however, we could hardly detect Nron expression in the proliferated intima SMCs in atherosclerotic lesions (Figure 1A). It is noteworthy that the fluorescence signal of Nron could be observed, although relatively weak, in the media of diseased vessels (Figure 1A). Further we examined the expression of Nron in the atherosclerotic mice. Consistently, Nron was highly expressed in normal aorta (aortic arch and thoracoabdominal aorta) and the expression was decreased in atherosclerotic aorta, whereas there was no change in the expression of Nron in the myocardium (Figure 1B). Also, we demonstrated that Nron was located in the cytoplasm of aortic smooth muscle cells (Figure 1C). Next we analyzed the dynamic changes of Nron in the progression of atherosclerosis. The level of Nron in the aorta of ApoE$^{-/-}$ mice decreased with age, and more markedly when mice were fed a western diet (WD), whereas it remained unchanged in wild type C57 mice either on a standard control diet (SCD) or on the WD (Figure S1A). These results indicated that the expression of Nron was closely related to disease severity rather than age or diet.

Nron overexpression in VSMC induces a highly characteristic architecture of more-vulnerable plaques

The reduction of Nron in the atherosclerotic artery prompted us to investigate whether there is a causal link between Nron and atherosclerosis. We treated ApoE$^{-/-}$ mice with adenovirus vector carrying Nron cDNA driven by the SM22α promoter (Ad-SM22-Nron) to induce overexpression (OE) of Nron in VSMCs. Time-course experiments revealed that transgene expression in aorta was evident at 1 week after intravenous injection of recombinant adenovirus vectors, and progressively declined to the base level subsequently (Figure S1B). The specificity of adenovirus with SM22α promoter to VSMCs *in vivo* was verified using immunofluorescence staining (Figure S1C). Considering the short-term expression of transgenes, adenovirus was administered every 2 weeks for 8 weeks before mice were sacrificed, as depicted in Figure S1D.

Body weights and plasma lipid profiles were unaffected by Nron gene transfer (Table S1). There were no significant differences in the lesion area, as determined by Oil Red O staining of thoracoabdominal aorta and aortic sinus, between Ad-SM22-Nron treated mice and control group (Ad-SM22-EV) (Figures 2A and 2B). Further the complexity of atherosclerotic plaques, in terms of macrophage (F4/80-positive) infiltration, smooth muscle cell (α-SMA positive) proliferation, collagen (Masson's Trichrome stain) content, fibrous cap and necrotic core areas, and the destruction of the elastic laminae (Verhoeff's Van Gieson stain), was assessed (Figures 2C and 2D). Compared with control mice, plaques of Nron OE mice contained a thinner VSMC-deficient fibrous cap with loose collagen and matrix overlying lipid-rich necrotic cores. In addition, the macrophage content was increased and the degradation of elastic fibers was more pronounced within lesions in Nron OE mice. These results suggest that Nron OE induces a highly characteristic architecture of more-vulnerable plaques.

Knockdown of Nron suppresses the development of atherosclerosis and increases the stability of atherosclerotic plaques

To achieve higher knockdown (KD) efficiency in the aorta, a recombinant adeno-associated virus (rAAV) vector carrying Nron shRNA (rAAV-shNron) is generated and applied. We examined the infection efficiencies of different vector types and found that intravenous injection of rAAV2/8 effectively knocked

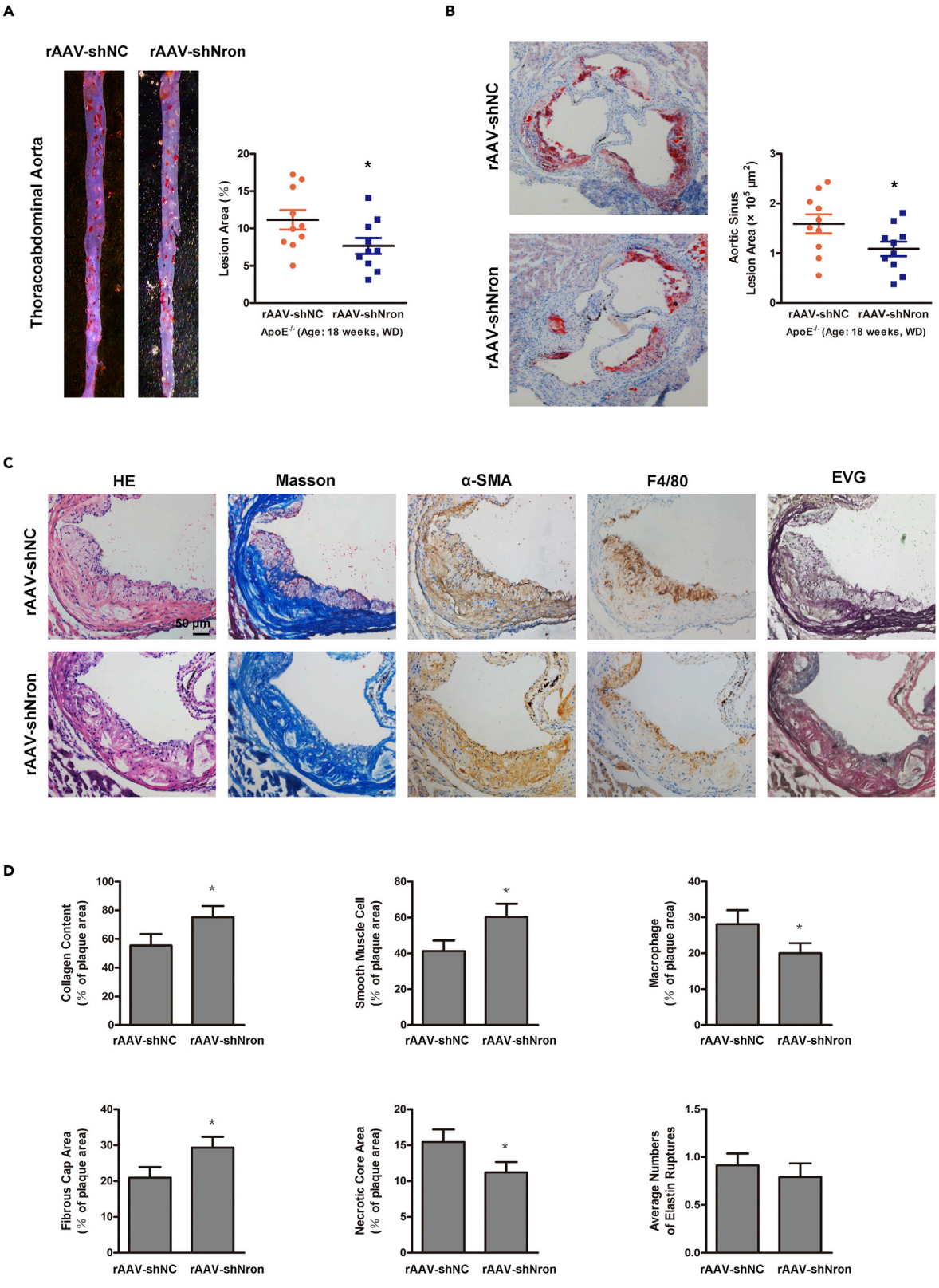
A
rAAV-shNC
rAAV-shNron
Thoracoabdominal Aorta
Lesion Area (%)
rAAV-shNC rAAV-shNron
ApoE-/- (Age: 18 weeks, WD)
B
rAAV-shNC
rAAV-shNron
Aortic Sinus Lesion Area (× 10^5 μm^2)
rAAV-shNC rAAV-shNron
ApoE-/- (Age: 18 weeks, WD)
C
HE
Masson
α-SMA
F4/80
EVG
rAAV-shNC
rAAV-shNron
50 μm
D
Collagen Content (% of plaque area)
Smooth Muscle Cell (% of plaque area)
Macrophage (% of plaque area)
Fibrous Cap Area (% of plaque area)
Necrotic Core Area (% of plaque area)
Average Numbers of Elastin Ruptures
rAAV-shNC rAAV-shNron

Figure 3. Knockdown of Nron suppresses the development of atherosclerosis and increases the stability of atherosclerotic plaques

6-Week male ApoE$^{-/-}$ mice were fed a western diet for 16 weeks. Mice received a single intravenous injection of adeno-associated virus 2/8 (rAAV-shNC or rAAV-shNron) after feeding for 4 weeks.

(A) Oil Red O staining of thoracoabdominal aorta, and lipid accumulation was quantified as percentage of total surface area of aorta.

(B) Images and quantification of Oil Red O staining in lesions of aortic sinus.

(C) Representative images of aortic sinus for H&E (HE), Masson's trichrome (Masson), Elastica van Gieson (EVG), smooth muscle cells (α-SMA), and macrophages (F4/80).

(D) Quantification of collagen content, fibrous cap area, necrotic core area, ruptures of elastic fibers, macrophage content, and smooth muscle cell content. Data are expressed as mean ± SEM (n = 12 per group). Statistical analysis was performed using Student's t test. *p <0.05 vs. rAAV-shNC group.

down the expression of Nron in the aorta of ApoE$^{-/-}$ mice, although not so efficiently as in the liver (Figures S1E and S1F). Because rAAV mediates long-term transgene expression *in vivo*, ApoE$^{-/-}$ mice were administered with rAAV2/8 at 10 weeks and were fed the WD continually for another 3 months before being sacrificed, as depicted in Figure S1G.

Oil Red O staining showed a significant decrease (29.4%) in lipid accumulation in the thoracoabdominal aorta of Nron KD mice compared with the control group (treated with rAAV-shNC) (Figure 3A). A consistent 31.6% decrease in lipid accumulation was also observed at the aortic sinus (Figure 3B). We next examined plaques for morphological features of plaque vulnerability (Figures 3C and 3D), and found a significant increase in collagen content and in fibrous cap area, as well as a higher proportion of smooth muscle cells in Nron KD mice compared with the control group. In addition, macrophage content and necrotic core area were considerably decreased within lesions from Nron KD mice. These results suggest that rAAV2/8 mediated Nron KD not only decreased the plaque area but also increased the plaque stability.

Noteworthy, after being fed an atherogenic diet for 4 months, Nron KD mice had slower weight gain and lower plasma triglyceride levels compared with the control group, while the cholesterol level tended to decrease but with no statistical significance (Table S2).

Nron binds to NFATc3 in VSMCs

As an important component of atherosclerotic lesions, VSMCs play critical roles in disease development. Moderate proliferation of VSMCs favors plaque stability in advanced lesions, and increased apoptosis rate leads to plaque rupture (Allahverdian et al., 2018; Grootaert et al., 2018). The fluorescence staining of aortic sinus lesions revealed decreased proliferative (Ki67-positive) VSMCs (Figures 4A and 4B) and increased apoptotic (Tunel-positive) VSMCs (Figures 4C and 4D) in Nron OE ApoE$^{-/-}$ mice compared with their control littermates. To gain insight into the molecular mechanism by which Nron regulates plaque stability and VSMC function, we performed a RNA pull-down assay followed by mass spectrometry (MS) analysis, and found that Interleukin enhancer-binding factor 2 (ILF2), a subunit of NFAT, associated with Nron in VSMCs (Figure 4E). The independent immunoblot assay further identified NFATc3, but not other NFAT proteins, as a specific Nron-binding protein (Figures 4F and S2). This finding was confirmed by an RNA immunoprecipitation (RIP) assay (Figure 4G).

NFATc3 is activated and translocates into the nucleus of VSMCs in atherosclerotic lesions

Although originally thought to be restricted to the regulation of immune function, different NFAT family members have since been shown to regulate different pathophysiological processes and are involved in various diseases (Liu et al., 2012; Schulz and Yutzey, 2004; Wu et al., 2007). We next examined the expression of NFAT proteins in normal and atherosclerotic vessels of mice. As shown by immunofluorescence staining (Figures 5A and S3), NFATc2, NFATc3, and NFATc4 were abundantly expressed in normal vessels and all localized in the cytoplasm of VSMCs, whereas NFATc1 was mainly localized in the myocardium. Remarkably, in the atherosclerotic lesions, NFATc3 was abundantly expressed in the fibrous cap and translocated from the cytoplasm to the nucleus, whereas NFATc2 and NFATc4 both retained in the cytoplasm. The consistent results were observed in the atherosclerotic plaques from humans (Figures S4A and S4B). We further examined the protein levels of NFATc3 in the aorta of animal models using western blot assay. NFATc3 was expressed in the cytoplasm and was barely detected in the nucleus in control C57 mice; however, the aorta form WD-fed ApoE$^{-/-}$ mice, which develop progressive atherosclerotic lesions, demonstrated an increase in the active form of NFATc3 (shown by faster migration within the gel), and a substantial increase of NFATc3 protein in the nucleus (Figures 5B and 5D). More significantly, Nron OE in VSMCs effectively inhibited the nuclear translocation of NFATc3 in the aorta of ApoE$^{-/-}$ mice (Figures 5C and 5E).

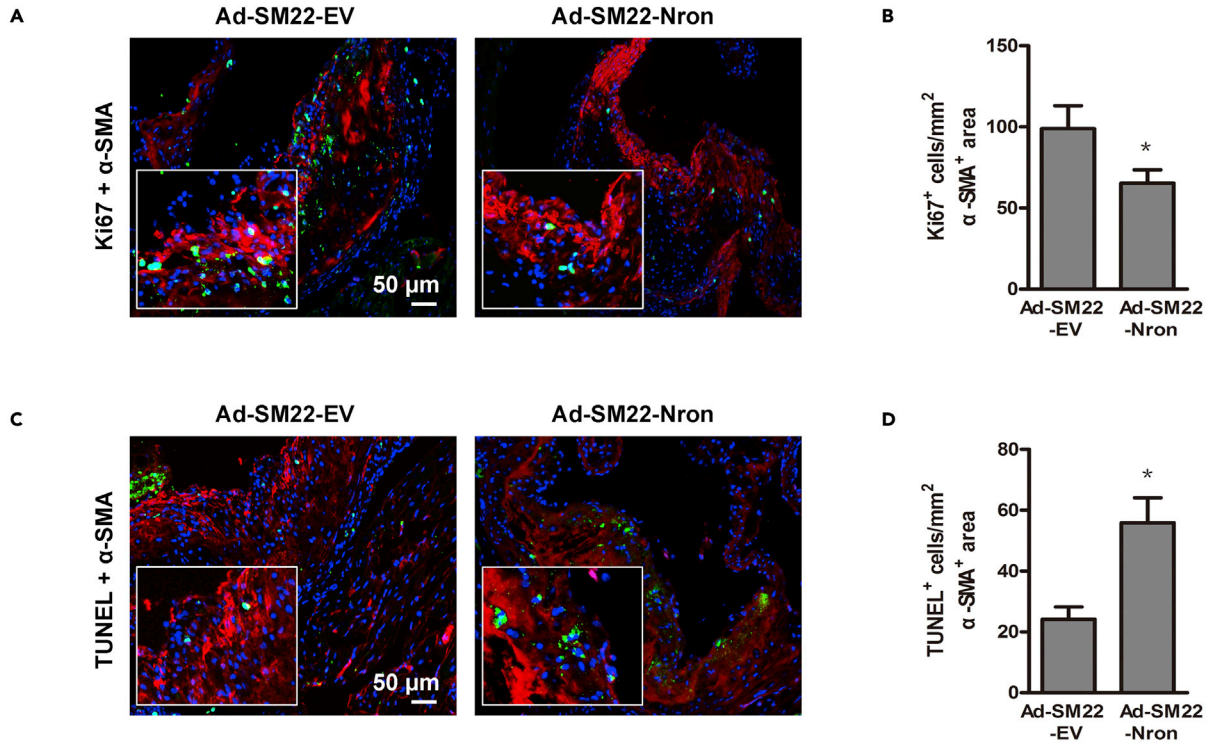
A
Ad-SM22-EV
Ad-SM22-Nron
Ki67 + α-SMA
50 μm
B
Ki67+ cells/mm2 α-SMA+ area
150
100
50
0
*
Ad-SM22 -EV
Ad-SM22 -Nron
C
Ad-SM22-EV
Ad-SM22-Nron
TUNEL + α-SMA
50 μm
D
TUNEL+ cells/mm2 α-SMA+ area
80
60
40
20
0
*
Ad-SM22 -EV
Ad-SM22 -Nron

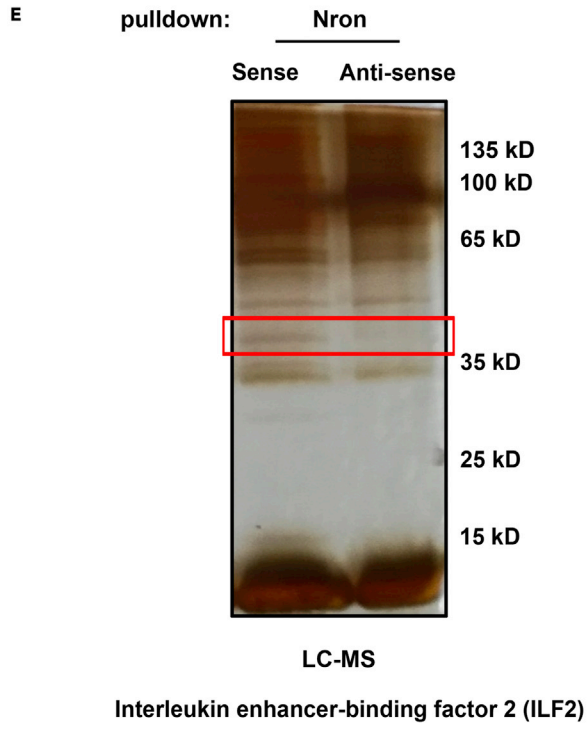
E
pulldown:
Nron
Sense
Anti-sense
135 kD
100 kD
65 kD
35 kD
25 kD
15 kD
LC-MS
Interleukin enhancer-binding factor 2 (ILF2)

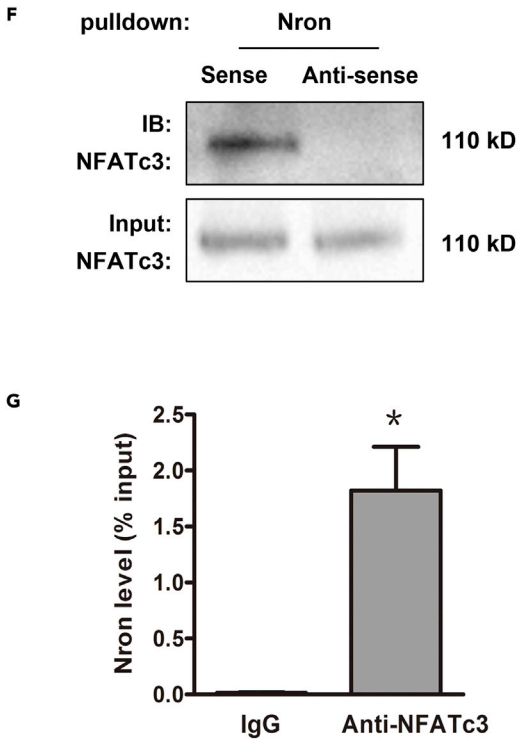
F
pulldown:
Nron
Sense
Anti-sense
IB:
NFATc3:
110 kD
Input:
NFATc3:
110 kD
G
Nron level (% input)
2.5
2.0
1.5
1.0
0.5
0.0
*
IgG
Anti-NFATc3

Figure 4. Nron binds to NFATc3 in VSMCs

(A–D) 6-week male ApoE$^{-/-}$ mice were fed a western diet for 16 weeks. Mice were intravenously administered with adenovirus (Ad-SM22-EV or Ad-SM22-Nron) every two weeks in the last 8 weeks before being sacrificed. Images (A) show Ki67 staining (green) of nuclei in sections of aortic sinus, and the number of proliferating cells was quantified (B) in VSMC-rich areas (red; α-SMA staining). Images (C) show TUNEL staining (green) of nuclei in sections of aortic sinus, and the number of apoptotic cells was quantified (D) in VSMC-rich areas (red; α-SMA staining). Data are expressed as mean ± SEM (n = 8 per group). *p <0.05 vs. Ad-SM22-EV group.

(E) Silver-stained SDS-PAGE gel analysis of proteins in VSMCs that are bound to biotinylated lncRNA-Nron. The highlighted regions were analyzed by mass spectrometry, identifying Interleukin enhancer-binding factor 2 (ILF2), a subunit of NFAT, as a protein unique to Nron.

(F) Immunoblotting analysis of proteins in VSMCs bound to biotinylated Nron using anti-NFATc3 antibody.

(G) RNA immunoprecipitation (RIP) analysis to determine the recovery of Nron in VSMCs using anti-NFATc3 antibody. IgG served as control. Data represent the mean ± SEM of three independent experiments. *p <0.05 vs. IgG group. Statistical analysis was performed using Student's t test.

Nron knockdown combined with ox-LDL treatment induces nuclear translocation of NFATc3 in VSMCs

Because Nron was proven to bind to NFATc3 in VSMCs, and its expression was decreased in the plaques, it is reasonable for us to speculate a direct regulation of Nron on NFATc3 activity. We transfected primary VSMCs with siRNA to induce Nron KD *in vitro* and treated them with ox-LDL. Neither ox-LDL treatment nor Nron KD induced NFATc3 nuclear translocation; however, when used together, we clearly observed a substantial accumulation of NFATc3 in the nucleus (Figure 6A). Western blot analysis further confirmed the results. NFATc3 was phosphorylated and retained in the cytoplasm, and Nron KD combined with ox-LDL led to the dephosphorylation and nuclear translocation of NFATc3 (Figures 6B and 6C). In line, the activity of NFAT-driven luciferase reporter was also increased in Nron KD VSMCs (Figure 6D). These findings suggest that the decrease in Nron expression coupled with ox-LDL challenge may be a reason for NFATc3 activation, and both of them are indispensable.

The effect of Nron KD on the proliferation, migration, and apoptosis of VSMC is dependent of NFATc3

Because Nron regulated the proliferation and apoptosis of VSMCs in atherosclerotic plaques of ApoE$^{-/-}$ mice, we tested whether this effect was mediated by the interaction of Nron with NFATc3. As assessed using an EdU assay, Nron KD combined with ox-LDL treatment promoted the proliferation of VSMCs cultured *in vitro*; however, this effect disappeared when NFATc3 was knocked down (Figures 7A and 7B). Moreover, the accelerating effect of Nron KD on the migration of VSMCs was also completely blocked by combined knockdown of NFATc3, as demonstrated by a transwell assay (Figures 7C and 7D). Next, the apoptosis of VSMCs was analyzed using the TUNEL assay. Nron KD caused a marked decrease in Tunel-positive VSMCs, and as expected, this anti-apoptotic effect was abrogated by knockdown of NFATc3 (Figures 7E and 7F). Collectively, these data indicated that the pro-proliferative and anti-apoptotic effects of Nron KD are dependent on the nuclear translocation and activation of NFATc3.

Nron contributes to neovascularization within the intima of atherosclerotic plaques

Neovascularization within the intima has been implicated as a possible contributor to the process by which an asymptomatic fibroatheromatous plaque becomes a lesion vulnerable to rupture, although the factors that trigger this process remain poorly understood (Perrotta et al., 2019; Sedding et al., 2018). To our surprise, we observed an increase in the number of microvessels staining positively for CD31 in the aortic sinus plaques of Nron OE ApoE$^{-/-}$ mice compared to the control group (Figure 8A). To determine the molecular and cellular mechanisms responsible for Nron actions in angiogenesis, we examined the expression of the angiogenic factors secreted by cultured VSMCs. Nron OE resulted in an increase in the mRNA levels of Vegfa and Vegfc in primary mouse VSMCs (Figure 8B), and Nron KD had a contrary effect (Figure 8E). Moreover, immunoblot analysis found that the protein level of VEGFA consistently changed (Figures 8C and 8F). The similar results were observed in a human aorta smooth muscle cell line T/G HA-VSMC (Figures S5A and S5B). Remarkably, Nron had no effects on the activity of NFAT-driven luciferase reporter without ox-LDL treatment (Figures 6D, 8D, and 8G). However, Nron OE significantly increased the luciferase activity of VEGFA promoter (Figure 8D), and Nron KD led to a reduction in the luciferase activity (Figure 8G). The results indicated that Nron modulates VEGFA expression at the transcriptional level independently of NFATc3. Consistently, as shown by immunohistochemistry assay, the expression of VEGFA was increased in the atherosclerotic plaques of Nron OE ApoE$^{-/-}$ mice (Figures S5C and S5D). Next, the tube formation assay was performed with mouse aortic endothelial cells (MAECs). We treated cultured MAECs with conditioned mediums from VSMCs, and measured the total branching lengths and branch points to assess EC

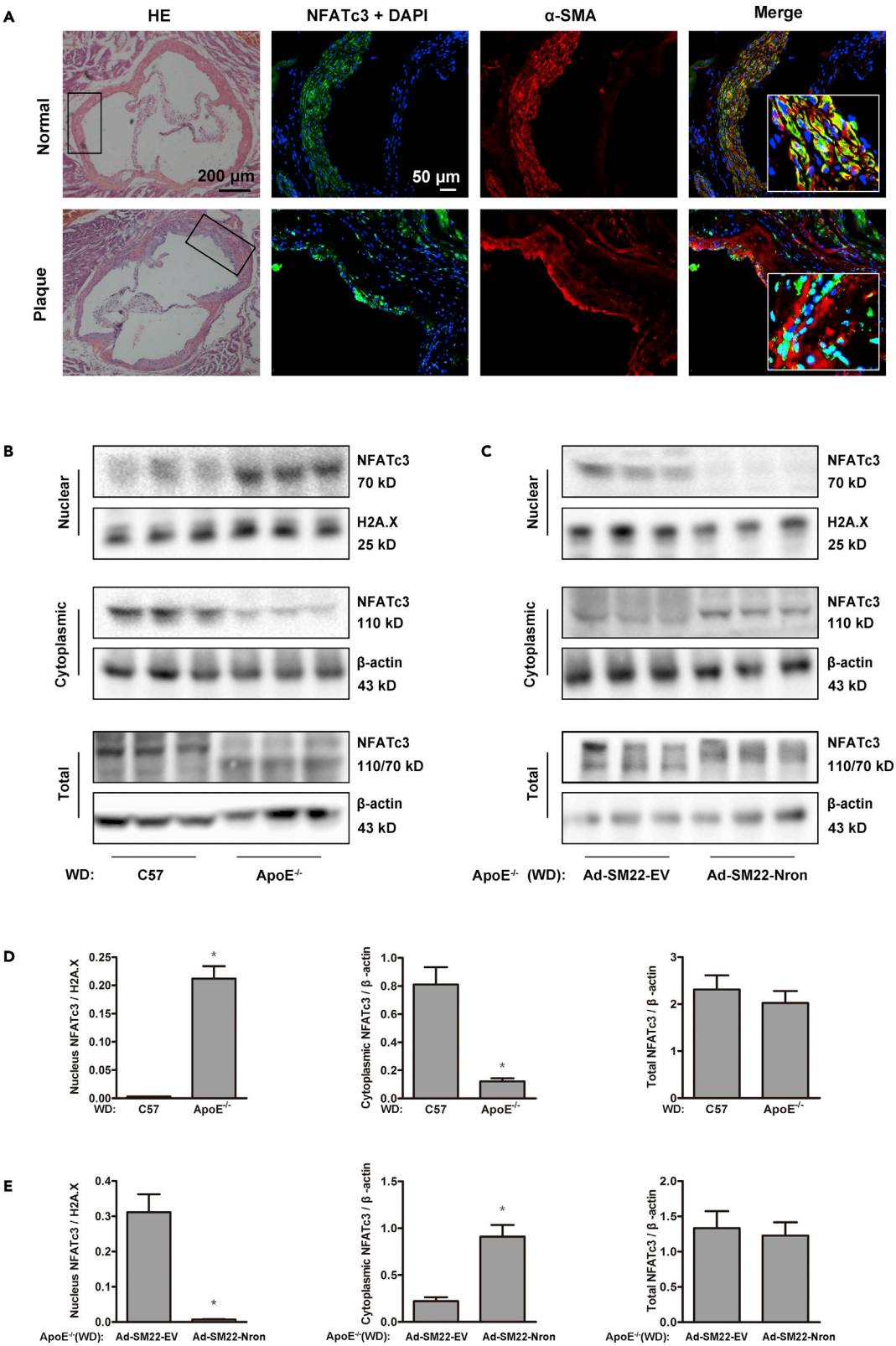
A
HE
NFATc3 + DAPI
α-SMA
Merge
Normal
Plaque
200 μm
50 μm
B
Nuclear
NFATc3
70 kD
H2A.X
25 kD
Cytoplasmic
NFATc3
110 kD
β-actin
43 kD
Total
NFATc3
110/70 kD
β-actin
43 kD
WD:
C57
ApoE-/-
C
Nuclear
NFATc3
70 kD
H2A.X
25 kD
Cytoplasmic
NFATc3
110 kD
β-actin
43 kD
Total
NFATc3
110/70 kD
β-actin
43 kD
ApoE-/- (WD):
Ad-SM22-EV
Ad-SM22-Nron
D
Nucleus NFATc3 / H2A.X
Cytoplasmic NFATc3 / β -actin
Total NFATc3 / β -actin
WD:
C57
ApoE-/-
E
Nucleus NFATc3 / H2A.X
Cytoplasmic NFATc3 / β -actin
Total NFATc3 / β -actin
ApoE-/-(WD):
Ad-SM22-EV
Ad-SM22-Nron

Figure 5. NFATc3 is activated and translocates into the nucleus of VSMCs in atherosclerotic lesions

(A) Immunofluorescence assay of NFATc3 in aortic sinus of C57BL/6 mice (normal) and ApoE$^{-/-}$ mice (plaque). For colocalization analysis, sections were co-stained for NFATc3 (green) and α-SMA (red; smooth muscle cell marker). DAPI was used for nucleus staining (blue).

(B) Representative immunoblot for NFATc3 expression in nucleus and cytoplasm in aorta of C57BL/6 mice and ApoE$^{-/-}$ mice fed with WD.

(C) Representative immunoblot for NFATc3 expression in nucleus and cytoplasm in aorta of WD-fed ApoE$^{-/-}$ mice infected with Ad-SM22-EV or Ad-SM22-Nron.

(D) Quantification of band density in panel (B).

(E) Quantification of band density in panel (C) Data are expressed as mean ± SEM (n = 6 per group). *p <0.05 vs. C57 group or Ad-SM22-EV group.

angiogenesis. The results showed that the total branching lengths and branch numbers in the group treated with medium from Nron OE VSMCs were significantly higher than in the group treated with control medium. However, knockdown of VEGFR2, the major receptor of VEGFA, in MAECs blocked the pro-angiogenic effect of Nron OE VSMCs (Figures 8H and 8I). These findings support the concept that VSMC-derived VEGFA, which is regulated by Nron, can function as a paracrine factor and contribute to the angiogenesis process.

DISCUSSION

A large body of evidence has indicated that lncRNAs are involved in atherosclerosis. In this study, decreased expression of lncRNA Nron was found specifically in VSMCs of atherosclerotic plaque samples. This led to the activation of NFATc3 to promote the proliferation and inhibit the apoptosis of VSMCs, and led to the inhibition of intra-plaque angiogenesis independently of NFATc3. All of these effects induce a highly characteristic architecture of more-stable atherosclerotic plaques. To the best of our knowledge, this is the first study that uncovers the role of Nron in VSMC function and in the development of atherosclerosis.

Nron was identified as a noncoding RNA repressor of the transcription factor NFAT. The NFAT family has five members, NFAT1 to NFAT5, of which all except NFAT5 are calcium regulated transcription factors (Crabtree and Clipstone, 1994; Lopez-Rodriguez et al., 1999; Timmerman et al., 1996). In resting T cells, NFATs are phosphorylated and retained in the cytoplasm. Following T cell antigen receptor (TCR) signals, NFAT proteins are dephosphorylated and translocate to the nucleus to activate gene expression (Crabtree and Clipstone, 1994; Timmerman et al., 1996). Nron was first reported to contribute to the assembly of a large RNA/protein complex (consists of a backbone of Nron and several proteins, including Tnpo1, Iqgap1, Cse1l, Ppp2r1a, and Psmd11), and function as a cytoplasmic trap for phosphorylated NFATc1 in T cells (Willingham et al., 2005). Subsequent work revealed that LRRK2 participates in the Nron complex and inhibits NFATc2 activity in macrophages (Liu et al., 2011). Moreover, a recent study reported that Nron suppresses NFATc3 nuclear transport and IL-12 expression in Ang II-treated atrial myocytes (the mechanism remains elusive) (Sun et al., 2019). It is possible that different cofactors determine the specificity of Nron to NFAT family in different cell types.

In the present study, we observed a substantial decrease in Nron expression accompanied by NFATc3 activation in atherosclerotic lesions, and provided evidence that Nron specifically associated with NFATc3 and regulated its nuclear trafficking in VSMCs. However, knockdown of Nron induced NFATc3 translocation only if cells were pretreated with ox-LDL. Cécile Mazière et al. have demonstrated that ox-LDL elicits an intracellular calcium rise and increases the binding activity of NFAT, thus regulating the expression of cytokine genes involved in the inflammatory response in T lymphocytes (Maziere et al., 2005). Our previous study also revealed that ox-LDL induces NFAT activation independently of Nron expression in macrophages, thus accelerating foam cell formation (Du et al., 2021). However, in the present study, ox-LDL could not induce NFATc3 nuclear translocation only when Nron was knocked down, possibly because of the higher expression level of Nron in VSMCs. Noteworthy, we did not observe the activation of other NFAT members in plaques, which suggested the functional heterogeneity of Nron and NFAT family in different cell types and diseases.

VSMCs play a pivotal role in atherogenesis. Classically, intimal VSMCs are considered to have a beneficial role by contributing to the fibrous cap and thereby stabilizing atherosclerotic plaque. Loss of VSMCs via apoptosis leads to fibrous cap thinning and promotes necrotic core formation. A role for NFAT in the migration and proliferation of VSMCs has been proposed in previous (Lipskaia et al., 2005; Liu et al., 2004, 2005). Here, we show that the combined knockdown of NFATc3 completely abrogated the

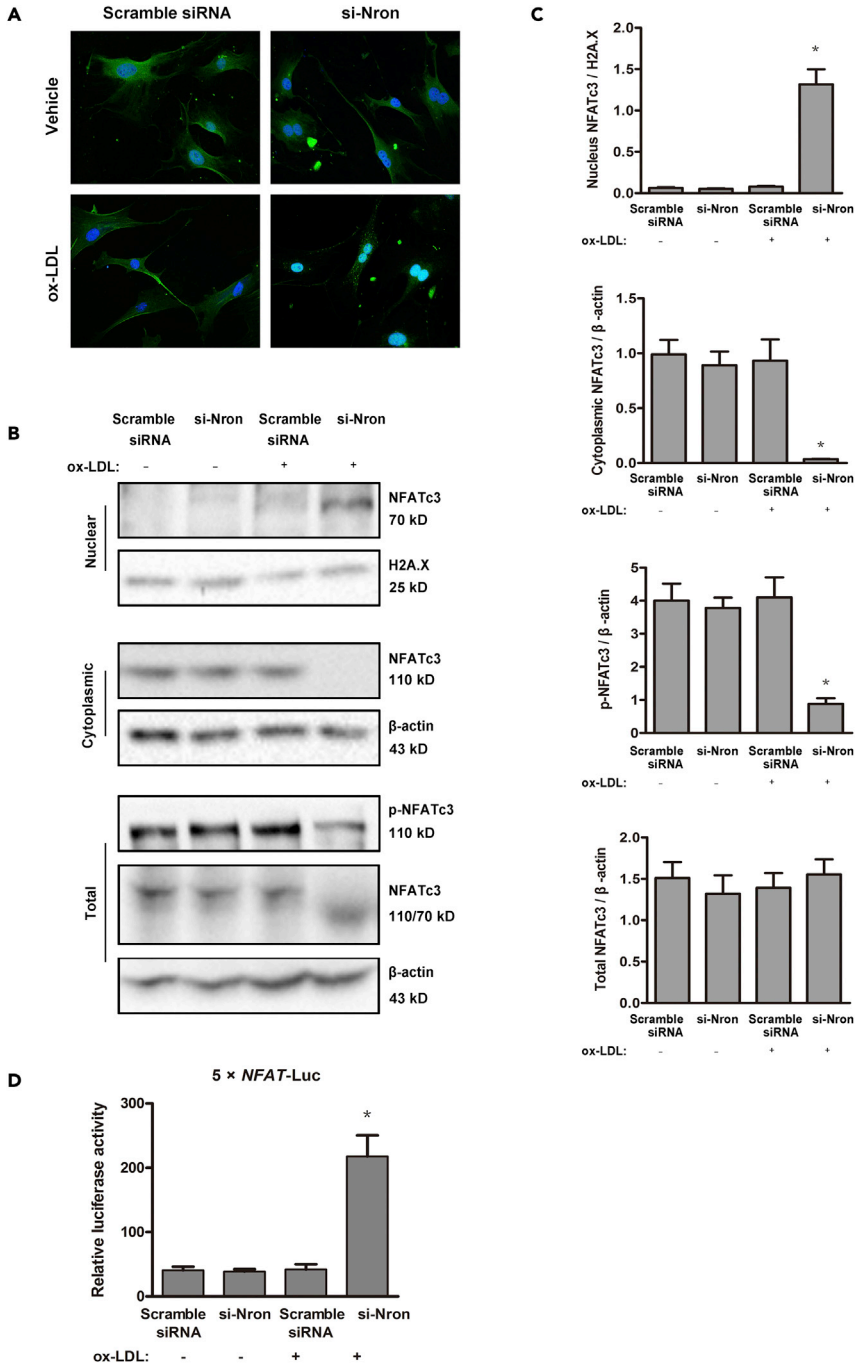

Figure 6. Nron knockdown combined with ox-LDL treatment induces nuclear translocation of NAFTc3 in VSMCs

Nron was knocked down in cultured mouse VSMCs with or without ox-LDL treatment.

(A) Immunofluorescence assay of NFATc3 (green) in VSMCs. DAPI was used for nucleus staining (blue).

(B) Representative immunoblot for NFATc3 expression in nucleus and cytoplasm of VSMCs.

(C) Quantification of band density in panel (B).

(D) The activity of NFAT-driven luciferase reporter was analyzed. Data were shown as mean ± SEM from three independent experiments. One-way ANOVA with Bonferroni test was used for data analysis. *p <0.05 vs. Scramble siRNA group.

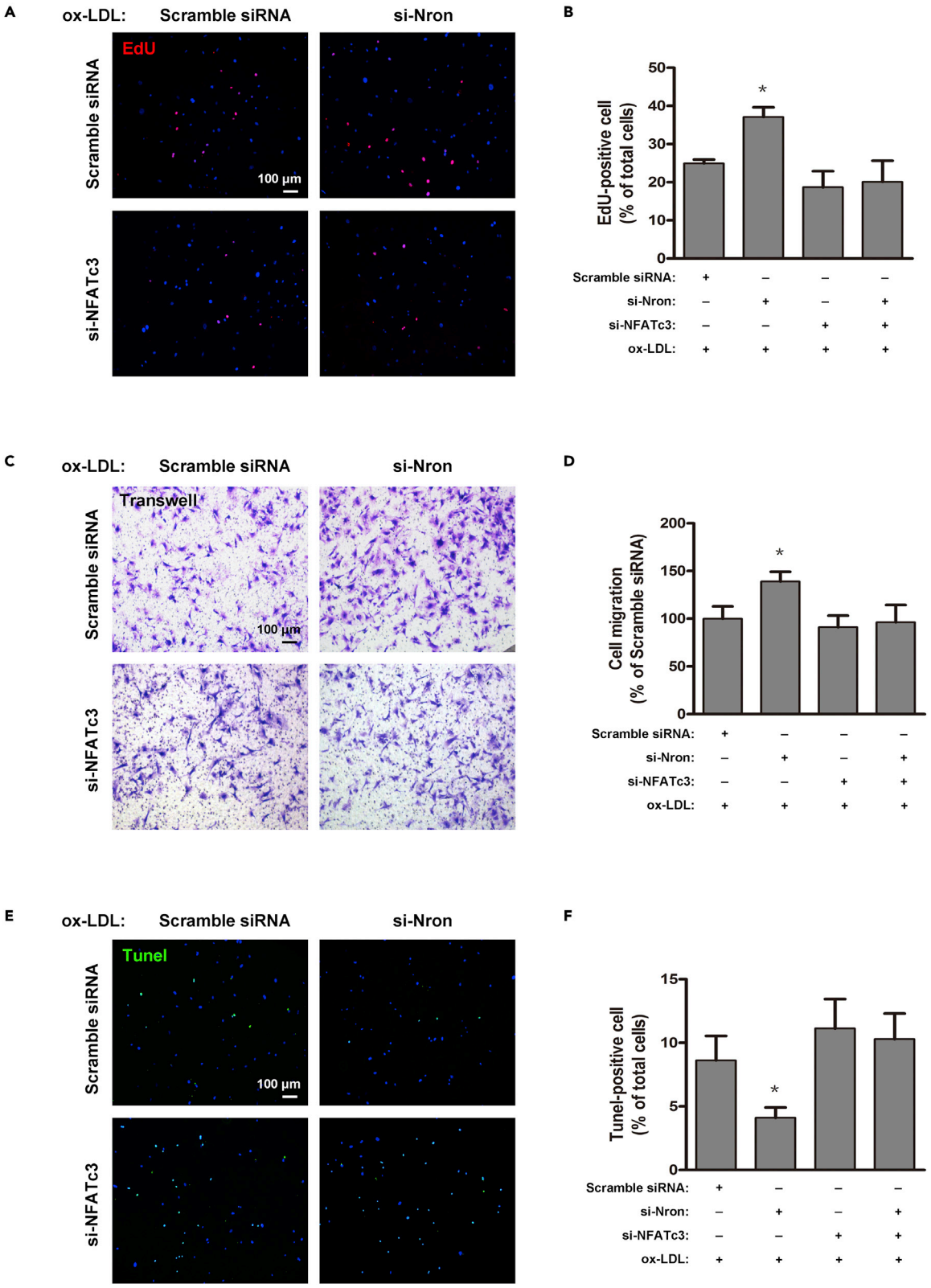
A
ox-LDL:
Scramble siRNA
si-Nron
EdU
Scramble siRNA
si-NFATc3
100 μm
B
EdU-positive cell (% of total cells)
50
40
30
20
10
0
*
Scramble siRNA: + – – –
si-Nron: – + – +
si-NFATc3: – – + +
ox-LDL: + + + +
C
ox-LDL:
Scramble siRNA
si-Nron
Transwell
Scramble siRNA
si-NFATc3
100 μm
D
Cell migration (% of Scramble siRNA)
200
150
100
50
0
*
Scramble siRNA: + – – –
si-Nron: – + – +
si-NFATc3: – – + +
ox-LDL: + + + +
E
ox-LDL:
Scramble siRNA
si-Nron
Tunel
Scramble siRNA
si-NFATc3
100 μm
F
Tunel-positive cell (% of total cells)
15
10
5
0
*
Scramble siRNA: + – – –
si-Nron: – + – +
si-NFATc3: – – + +
ox-LDL: + + + +

Figure 7. The effect of Nron KD on the proliferation, migration, and apoptosis of VSMC is dependent on NFATc3 activation

Nron or NFATc3 was knocked down in cultured mouse VSMCs treated with ox-LDL.

(A and B) VSMC proliferation was evaluated by the EdU assay.

(C and D) VSMC migration was examined using a transwell assay.

(E and F) VSMC apoptosis was evaluated by TUNEL staining. Data represent the mean ± SEM of three independent experiments. One-way ANOVA with Bonferroni test was used for data analysis. *p <0.05 vs. Scramble siRNA group.

proliferative and anti-apoptotic effects of Nron KD in VSMCs challenged with ox-LDL. It provided direct evidence for the involvement of Nron-NFATc3 interaction in the regulation of VSMC behavior.

Microvessels are rarely present in the healthy intima of the vessel wall but are usually observed in pathological conditions such as atherosclerosis. Intra-plaque angiogenesis is an important trigger for plaque progression, and also associated with plaque erosion, hemorrhage, and coronary thrombosis (Perrotta et al., 2019; Sedding et al., 2018). Because the newly formed vessels growing into the plaque are immature, they are inherently leaky, permitting inflammatory cell infiltration and influx of blood constituents (including erythrocytes and blood platelets), and making it an important hallmark of plaque instability (Kaartinen et al., 1996). VEGFA, which is released by various cell types including SMCs, ECs, and macrophages, is a potent initiator of neovascularization. VEGFA contributes to the maintenance and regeneration of arterial endothelium in physiological conditions; however, elevated VEGFA within advanced atherosclerotic plaques clearly leads to highly permeable and leaky microvessels, which fail to mature properly (Inoue et al., 1998; Pelisek et al., 2012). In the present study, we observed more microvessels in plaques of Nron OE mice, and provided evidence that Nron promotes the expression of VEGFA in VSMCs. VEGFA secreted by VSMCs functions as a paracrine factor and contributes to EC angiogenesis within the intima of atherosclerotic plaques. This may be one of the important factors to induce plaque instability. Remarkably, Nron modulates VEGFA expression at the transcriptional level, and the effect is independent of NFATc3. More research is needed to clarify the detail mechanism.

To explore Nron functions in VSMCs during atherosclerosis development, adenovirus vector driven by the SM22α promoter was used to manipulate Nron expression in the aorta. Besides, we successfully used rAAV2/8 vector carrying Nron shRNA delivered by tail vein injection to obtain stable knockdown of Nron in the aorta, although this effect is not VSMC-specific. Surprisingly, rAAV2/8 mediated Nron KD not only increased the plaque stability but significantly decreased the plaque area of aorta and aortic sinus (Nron OE in VSMC had no effect on the plaque area). It is noteworthy that Nron KD mice had an improved serum lipid profile and lower weight again. Because rAAV2/8-shNron also caused a significant decrease in Nron expression in the liver, it is quite possible that Nron KD in the liver could improve energy metabolism, and thereby restraining the development of atherosclerosis in another way. This finding indicates a potential role of Nron in other metabolic diseases, which is worth our further research. Besides, it might make more sense and be taken into account to employ conditional knockout or transgenic mice in our future studies to elucidate the specific role of Nron in different cell types involved in the pathogenesis of atherosclerosis.

Although the change of Nron expression has been observed in various diseases, especially in malignant tumors (Xiong et al., 2020; Yao et al., 2018), there is no report on the regulation of Nron expression or hypotheses up to now. In our study, the expression of Nron is decreased in atherosclerosis-bearing aortas, and reversing its expression induces a highly characteristic architecture of more-vulnerable plaques. We speculate that Nron may play a role in protective, compensative, and negative feedback regulation in atherosclerosis, while the mechanism needs further investigation.

In conclusion, the decreased expression of lncRNA Nron increases the stability of atherosclerotic plaques through regulating VSMC function and inhibiting neovascularization in advanced lesions. The present study provides an important clue to help elucidate the pathogenesis of atherosclerosis and implicates Nron as a potential therapeutic target for atherosclerosis.

Limitations of study

Adenovirus vector and rAAV2/8 vector were used to manipulate Nron expression in our study, but the effect was not very specific for certain cell types. We observed improved metabolic indexes in Nron KD mice and this indicates a comprehensive, but not VSMC-specific, role of Nron in atherosclerosis. More related detail has yet to be determined.

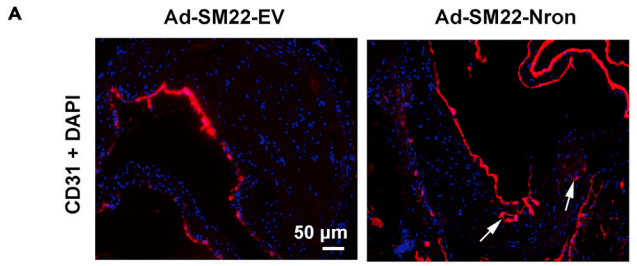

	Aortic sinus plaque, n	Neovascularization (+)*	P†
Ad-SM22-EV	26	1 (3.8 %)	
Ad-SM22-Nron	24	5 (20.8 %)	0.014

* Plaques with ≥ 1 intimal capillary were counted positive

† Chi-square test with Yate's correction

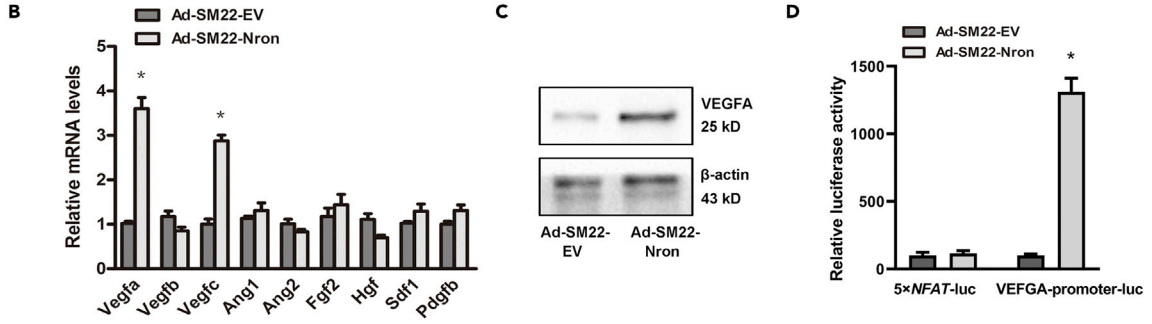

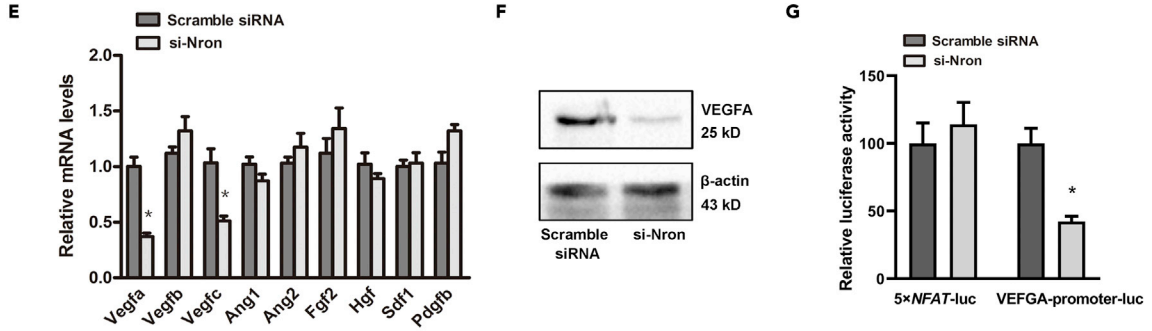

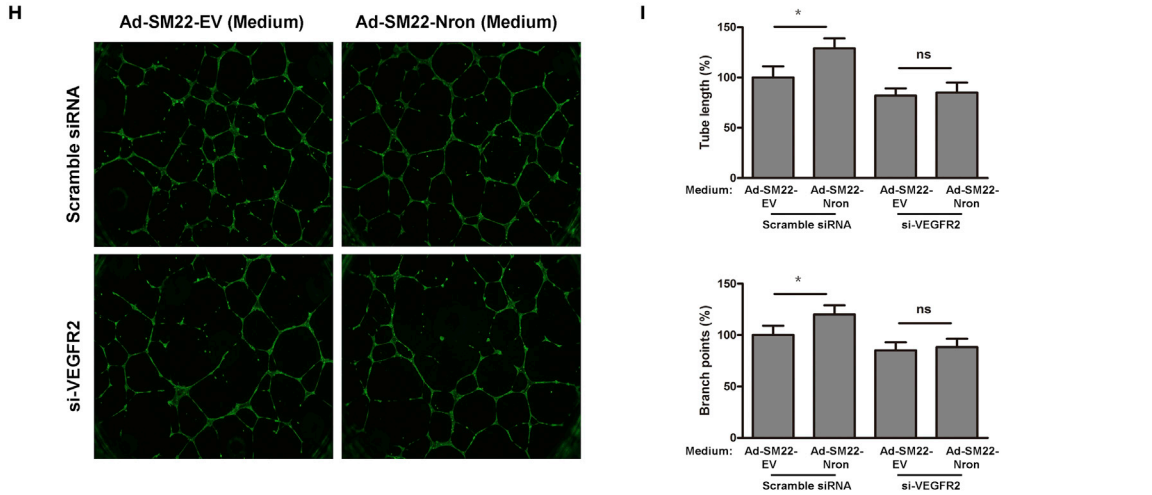

Figure 8. Nron contributes to neovascularization in the atherosclerotic plaques

(A) 6-week male ApoE$^{-/-}$ mice were fed a western diet for 16 weeks. Mice were intravenously administered with adenovirus (Ad-SM22-EV or Ad-SM22-Nron) every two weeks in the last 8 weeks before being sacrificed. *Left panel*: Sections of the aortic sinus were subjected to immunofluorescence staining with antibodies against CD31. Positive staining of the endothelium on the lumen and in adventitial capillaries served as an internal control. The arrowhead indicates the neovascularization in the plaques. *Right panel*: Quantitative data of the total number of vasa vasorum numbers in the plaques.

(B–D) Mouse VSMCs cultured *in vitro* was infected with Ad-SM22-EV or Ad-SM22-Nron. The mRNA levels of pro-angiogenic factors (B), the protein level of VEGFA (C), and the activities of NFAT-driven or VEGFA promoter luciferase reporter (D) were determined.

(E–G) Mouse VSMCs cultured *in vitro* were transfected with si-Nron or scramble siRNA. The mRNA levels of pro-angiogenic factors (E), the protein level of VEGFA (F), and the activities of NFAT-driven and VEGFA promoter luciferase reporter (G) were determined.

(H and I) Tube formation was determined in mouse aortic endothelial cells (MAECs). MAECs were transfected with VEGFR2 siRNA or scramble siRNA, and then incubated with medium from Nron OE VSMCs or control VSMCs. Representative images (H) and quantitative data (I) of branch length and branch points were presented. Data were shown as mean ± SEM from three independent experiments. Student's t test was used for panel (B, D, E, and G). One-way ANOVA with Bonferroni test was used for panel (I) *p <0.05.

STAR★METHODS

Detailed methods are provided in the online version of this paper and include the following:

- KEY RESOURCES TABLE
- RESOURCE AVAILABILITY
  - Lead contact
  - Materials availability
  - Data and code availability
- EXPERIMENTAL MODEL AND SUBJECT DETAILS
  - Cell cultures
  - Animals
  - Human atherosclerotic tissues
- METHOD DETAILS
  - Generation of recombinant adenovirus and adeno-associated virus
  - Histological analysis and quantification of atherosclerotic lesions
  - RNA fluorescence *in situ* hybridization
  - Immunofluorescence
  - RNA extraction and qRT-PCR
  - Western blot
  - RNA pull-down and mass spectrometry
  - RNA immunoprecipitation
  - VSMC proliferation assay
  - VSMC migration assay
  - VSMC Tunel assay
  - Tube formation assay
- QUANTIFICATION AND STATISTICAL ANALYSIS

SUPPLEMENTAL INFORMATION

Supplemental information can be found online at https://doi.org/10.1016/j.isci.2022.103978.

ACKNOWLEDGMENTS

This work was supported by the National Natural Science Foundation of China [82071794 to M.D., 91949201 and 81830014 to K.H.].

AUTHORS CONTRIBUTIONS

M.D. and K.H. designed the experiments and wrote the manuscript. M.D., C.M., Liuye Yang., B.L., and Z.Z. performed the experiments. Liu Yang. and F.Z. analyzed the data and generated data figures. J.P. and D.H. contributed reagents/materials/analysis tools. All authors contributed to the refinement of the study and reviewed and approved the final version of the manuscript. Liu Yang. and F.Z. verified the underlying data.

DECLARATION OF INTERESTS

The authors declare no potential conflicts of interest.

Received: September 27, 2021
Revised: December 31, 2021
Accepted: February 21, 2022
Published: March 18, 2022

REFERENCES

Allahverdian, S., Chaabane, C., Boukais, K., Francis, G.A., and Bochaton-Piallat, M.L. (2018). Smooth muscle cell fate and plasticity in atherosclerosis. Cardiovasc. Res. *114*, 540–550. https://doi.org/10.1093/cvr/cvy022.

Clarke, M.C., Figg, N., Maguire, J.J., Davenport, A.P., Goddard, M., Littlewood, T.D., and Bennett, M.R. (2006). Apoptosis of vascular smooth muscle cells induces features of plaque vulnerability in atherosclerosis. Nat. Med. *12*, 1075–1080. https://doi.org/10.1038/nm1459.

Crabtree, G.R., and Clipstone, N.A. (1994). Signal transmission between the plasma membrane and nucleus of T lymphocytes. Annu. Rev. Biochem. *63*, 1045–1083. https://doi.org/10.1146/annurev.bi.63.070194.005145.

de Nooijer, R., Bot, I., von der Thusen, J.H., Leeuwenburgh, M.A., Overkleeft, H.S., Kraaijeveld, A.O., Dorland, R., van Santbrink, P.J., van Heiningen, S.H., Westra, M.M., et al. (2009). Leukocyte cathepsin S is a potent regulator of both cell and matrix turnover in advanced atherosclerosis. Arterioscler. Thromb. Vasc. Biol. *29*, 188–194. https://doi.org/10.1161/ATVBAHA.108.181578.

Du, M., Yang, L., Liu, B., Mao, X., Liang, M., and Huang, K. (2021). Inhibition of NFAT suppresses foam cell formation and the development of diet-induced atherosclerosis. FASEB J. *35*, e21951. https://doi.org/10.1096/fj.202100947R.

Glass, C.K., and Witztum, J.L. (2001). Atherosclerosis. the road ahead. Cell *104*, 503–516. https://doi.org/10.1016/s0092-8674(01)00238-0.

Grootaert, M.O.J., Moulis, M., Roth, L., Martinet, W., Vindis, C., Bennett, M.R., and De Meyer, G.R.Y. (2018). Vascular smooth muscle cell death, autophagy and senescence in atherosclerosis. Cardiovasc. Res. *114*, 622–634. https://doi.org/10.1093/cvr/cvy007.

Gupta, K., Radotra, B.D., Banerjee, A.K., and Nijhawan, R. (2004). Quantitation of angiogenesis and its correlation with vascular endothelial growth factor expression in astrocytic tumors. Anal. Quant. Cytol. Histol. *26*, 223–229.

Holdt, L.M., Kohlmaier, A., and Teupser, D. (2019). Long noncoding RNAs of the arterial wall as therapeutic agents and targets in atherosclerosis. Thromb. Haemost. *119*, 1222–1236. https://doi.org/10.1055/s-0039-1692680.

Imam, H., Bano, A.S., Patel, P., Holla, P., and Jameel, S. (2015). The lncRNA NRON modulates HIV-1 replication in a NFAT-dependent manner and is differentially regulated by early and late viral proteins. Sci. Rep. *5*, 8639. https://doi.org/10.1038/srep08639.

Inoue, M., Itoh, H., Ueda, M., Naruko, T., Kojima, A., Komatsu, R., Doi, K., Ogawa, Y., Tamura, N., Takaya, K., et al. (1998). Vascular endothelial growth factor (VEGF) expression in human coronary atherosclerotic lesions: possible pathophysiological significance of VEGF in progression of atherosclerosis. Circulation *98*, 2108–2116. https://doi.org/10.1161/01.cir.98.20.2108.

Kaartinen, M., Penttila, A., and Kovanen, P.T. (1996). Mast cells accompany microvessels in human coronary atheromas: implications for intimal neovascularization and hemorrhage. Atherosclerosis *123*, 123–131. https://doi.org/10.1016/0021-9150(95)05794-3.

Kraczkowska, W., and Jagodzinski, P.P. (2019). The long non-coding RNA landscape of atherosclerotic plaques. Mol. Diagn. Ther. *23*, 735–749. https://doi.org/10.1007/s40291-019-00427-9.

Li, J., Chen, C., Ma, X., Geng, G., Liu, B., Zhang, Y., Zhang, S., Zhong, F., Liu, C., Yin, Y., et al. (2016). Long noncoding RNA NRON contributes to HIV-1 latency by specifically inducing tat protein degradation. Nat. Commun. *7*, 11730. https://doi.org/10.1038/ncomms11730.

Lipskaia, L., del Monte, F., Capiod, T., Yacoubi, S., Hadri, L., Hours, M., Hajjar, R.J., and Lompre, A.M. (2005). Sarco/endoplasmic reticulum Ca2+-ATPase gene transfer reduces vascular smooth muscle cell proliferation and neointima formation in the rat. Circ. Res. *97*, 488–495. https://doi.org/10.1161/01.RES.0000180663.42594.aa.

Liu, Z., Dronadula, N., and Rao, G.N. (2004). A novel role for nuclear factor of activated T cells in receptor tyrosine kinase and G protein-coupled receptor agonist-induced vascular smooth muscle cell motility. J. Biol. Chem. *279*, 41218–41226. https://doi.org/10.1074/jbc.M406917200.

Liu, Z., Zhang, C., Dronadula, N., Li, Q., and Rao, G.N. (2005). Blockade of nuclear factor of activated T cells activation signaling suppresses balloon injury-induced neointima formation in a rat carotid artery model. J. Biol. Chem. *280*, 14700–14708. https://doi.org/10.1074/jbc.M500322200.

Liu, Z., Lee, J., Krummey, S., Lu, W., Cai, H., and Lenardo, M.J. (2011). The kinase LRRK2 is a regulator of the transcription factor NFAT that modulates the severity of inflammatory bowel disease. Nat. Immunol. *12*, 1063–1070. https://doi.org/10.1038/ni.2113.

Liu, Q., Chen, Y., Auger-Messier, M., and Molkentin, J.D. (2012). Interaction between NFkappaB and NFAT coordinates cardiac hypertrophy and pathological remodeling. Circ. Res. *110*, 1077–1086. https://doi.org/10.1161/CIRCRESAHA.111.260729.

Lopez-Rodriguez, C., Aramburu, J., Rakeman, A.S., and Rao, A. (1999). NFAT5, a constitutively nuclear NFAT protein that does not cooperate with Fos and Jun. Proc. Natl. Acad. Sci. U S A *96*, 7214–7219. https://doi.org/10.1073/pnas.96.13.7214.

Lusis, A.J. (2000). Atheroscler. Nature *407*, 233–241. https://doi.org/10.1038/35025203.

Maziere, C., Morliere, P., Massy, Z., Kamel, S., Louandre, C., Conte, M.A., and Maziere, J.C. (2005). Oxidized low-density lipoprotein elicits an intracellular calcium rise and increases the binding activity of the transcription factor NFAT. Free Radic. Biol. Med. *38*, 472–480. https://doi.org/10.1016/j.freeradbiomed.2004.10.028.

Niu, L., Fan, Q., Yan, M., and Wang, L. (2019). LncRNA NRON down-regulates lncRNA snaR and inhibits cancer cell proliferation in TNBC. Biosci. Rep. *39*. https://doi.org/10.1042/BSR20190468.

Pelisek, J., Well, G., Reeps, C., Rudelius, M., Kuehnl, A., Culmes, M., Poppert, H., Zimmermann, A., Berger, H., and Eckstein, H.H. (2012). Neovascularization and angiogenic factors in advanced human carotid artery stenosis. Circ. J. *76*, 1274–1282. https://doi.org/10.1253/circj.cj-11-0768.

Perrotta, P., Emini Veseli, B., Van der Veken, B., Roth, L., Martinet, W., and De Meyer, G.R.Y. (2019). Pharmacological strategies to inhibit intraplaque angiogenesis in atherosclerosis. Vasc. Pharmacol. *112*, 72–78. https://doi.org/10.1016/j.vph.2018.06.014.

Schulz, R.A., and Yutzey, K.E. (2004). Calcineurin signaling and NFAT activation in cardiovascular and skeletal muscle development. Dev. Biol. *266*, 1–16. https://doi.org/10.1016/j.ydbio.2003.10.008.

Sedding, D.G., Boyle, E.C., Demandt, J.A.F., Sluimer, J.C., Dutzmann, J., Haverich, A., and Bauersachs, J. (2018). Vasa vasorum angiogenesis: key player in the initiation and progression of atherosclerosis and potential target for the treatment of cardiovascular disease. Front. Immunol. *9*, 706. https://doi.org/10.3389/fimmu.2018.00706.

Sharma, S., Findlay, G.M., Bandukwala, H.S., Oberdoerffer, S., Baust, B., Li, Z., Schmidt, V., Hogan, P.G., Sacks, D.B., and Rao, A. (2011). Dephosphorylation of the nuclear factor of activated T cells (NFAT) transcription factor is regulated by an RNA-protein scaffold complex. Proc. Natl. Acad. Sci. U S A *108*, 11381–11386. https://doi.org/10.1073/pnas.1019711108.

Sun, F., Guo, Z., Zhang, C., Che, H., Gong, W., Shen, Z., Shi, Y., and Ge, S. (2019). LncRNA NRON alleviates atrial fibrosis through suppression of M1 macrophages activated by atrial myocytes. Biosci. Rep. *39*. https://doi.org/10.1042/BSR20192215.

Timmerman, L.A., Clipstone, N.A., Ho, S.N., Northrop, J.P., and Crabtree, G.R. (1996). Rapid shuttling of NF-AT in discrimination of Ca2+

signals and immunosuppression. Nature *383*, 837–840. https://doi.org/10.1038/383837a0.

Willingham, A.T., Orth, A.P., Batalov, S., Peters, E.C., Wen, B.G., Aza-Blanc, P., Hogenesch, J.B., and Schultz, P.G. (2005). A strategy for probing the function of noncoding RNAs finds a repressor of NFAT. Science *309*, 1570–1573. https://doi.org/10.1126/science.1115901.

Wu, H., Peisley, A., Graef, I.A., and Crabtree, G.R. (2007). NFAT signaling and the invention of vertebrates. Trends Cell Biol. *17*, 251–260. https://doi.org/10.1016/j.tcb.2007.04.006.

Xiong, T., Huang, C., Li, J., Yu, S., Chen, F., Zhang, Z., Zhuang, C., Li, Y., Huang, X., Ye, J., et al. (2020). LncRNA NRON promotes the proliferation, metastasis and EMT process in bladder cancer. J. Cancer *11*, 1751–1760. https://doi.org/10.7150/jca.37958.

Yan, Y., Song, D., Wu, J., and Wang, J. (2020). Long non-coding RNAs link oxidized low-density lipoprotein with the inflammatory response of macrophages in atherogenesis. Front. Immunol. *11*, 24. https://doi.org/10.3389/fimmu.2020.00024.

Yao, Z., Xiong, Z., Li, R., Liang, H., Jia, C., and Deng, M. (2018). Long non-coding RNA NRON is downregulated in HCC and suppresses tumour cell proliferation and metastasis. Biomed. Pharmacother. *104*, 102–109. https://doi.org/10.1016/j.biopha.2018.05.006.

Zhang, Z., Salisbury, D., and Sallam, T. (2018). Long noncoding RNAs in atherosclerosis: JACC review topic of the week. J. Am. Coll. Cardiol. *72*, 2380–2390. https://doi.org/10.1016/j.jacc.2018.08.2161.

STAR★METHODS

KEY RESOURCES TABLE

REAGENT or RESOURCE	SOURCE	IDENTIFIER
Antibodies		
Rabbit polyclonal to F4/80	Abcam	Cat#ab100790
Mouse monoclonal [1A4] to alpha smooth muscle Actin	Abcam	Cat#ab240654
Mouse monoclonal [VG-1] to VEGFA	Abcam	Cat#ab1316
Rabbit monoclonal [EPR17259] to CD31	Abcam	Cat#ab182981
Rabbit polyclonal to NFATC1	Abcam	Cat#ab25916
Mouse monoclonal [4G6-G5] to NFATC2	Santa Cruz	Cat#sc-7296
Mouse monoclonal [F-1] to NFATC3	Santa Cruz	Cat#sc-8405
Rabbit polyclonal to NFATC4	Abcam	Cat#ab99431
Goat anti-Rabbit IgG (H + L) Cross-Adsorbed ReadyProbes™ Secondary Antibody, Alexa Fluor 488	Molecular probes	Cat#R37116
Goat anti-Mouse IgG (H + L) Cross-Adsorbed ReadyProbes™ Secondary Antibody, Alexa Fluor 594	Molecular probes	Cat#R37121
Bacterial and virus strains		
pAV-SM22alpha-MCS-SV40-EGFP	Shanghai GeneChem	N/A
pAAV-U6-shRNA-CAG-EGFP	Shanghai GeneChem	N/A
Chemicals, peptides, and recombinant proteins		
ABC HRP Mini-PLUS Kit	Vector Laboratories	Cat#PK-850275
TRIzol reagent	Takara Bio	Cat#D9108A
PrimeScript™ RT Master Mix	Takara Bio	Cat#RR036A
One Step TB Green® PrimeScript™ RT-PCR Kit	Takara Bio	Cat#RR066A
Protease Inhibitor Cocktail	Sigma-Aldrich	Cat#P8340
Pierce™ Rapid Gold BCA Protein Assay Kit	Thermo Scientific	Cat#A53226
Collagenase type II	Worthington Biochemical Corp	Cat#LS004176
Collagenase type I	Sigma	Cat#C-0130
Elastase	Sigma	Cat#E−0127
RNeasy Mini Kit	QIAGEN	Cat#74106
T7 RNA polymerase	Invitrogen	Cat#18033019
Critical commercial assays		
Pierce™ magnetic RNA–protein pull-down kit	Thermo Fisher Scientific	Cat#20164
Pierce silver stain kit	Thermo Fisher Scientific	Cat#24612
Cell-Light EdU Apollo 567 *In Vitro* Kit	RiboBio	Cat#C10310
One-Step TUNEL Apoptosis Kit	RiboBio	Cat#C11026
Experimental models: Organisms/strains		
C57BL/6J Mice	Beijing Hfk Bioscience	http://www.hfkbio.com/
B6-ApoE tm1 Mice (ApoE)	Beijing Hfk Bioscience	http://www.hfkbio.com/
Oligonucleotides		
qPCR primers	TSINGKE Biological Technology	See Table S1

(*Continued on next page*)

Continued

REAGENT or RESOURCE	SOURCE	IDENTIFIER
miRCURY LNA™ detection probe (Nron)	Exiqon	5′–3′/5DigN/ TAAAGGAGCAGTGGTAGAAACA/3DigN/
Software and algorithms		
GraphPad Prism 5	GraphPad Software Inc	https://www.graphpad.com/
Image Pro Plus	Media Cybernetics	N/A
ImageJ Software	National Institutes of Health	https://imagej.nih.gov
Axiovision software 4.8	ZEISS	https://www.directindustry.com/

RESOURCE AVAILABILITY

Lead contact

Further information and requests for resources and reagents should be directed to and will be fulfilled by the lead contact, Meng Du (d201378184@alumni.hust.edu.cn).

Materials availability

All unique/stable reagents generated in this study are available from the lead contact upon request.

Data and code availability

- All data reported in this paper will be shared by the lead contact upon request.
- This paper does not report original code.
- Any additional information required to reanalyze the data reported in this paper is available from the lead contact upon request.

EXPERIMENTAL MODEL AND SUBJECT DETAILS

Cell cultures

Primary VSMCs were obtained from 6 to 8-week-old C57BL/6 male mouse aortas using collagenase-elastase digestion as follows: aortas were excised, washed in phosphatebuffered saline, and incubated in DMEM (Invitrogen) containing 1 mg/mL of Collagenase type II (LS004176, Worthington Biochemical Corp) for 10 to 15 min. Then, under microscopic guidance, the vessels were stripped of adventitia, minced with scissors and digested with Collagenase type I (C-0130, Sigma) 0.5 mg/mL and Elastase type III (E−0127, Sigma) 0.125 mg/mL in serum-free DMEM with antibiotics at 37°C until most cells were in suspension. The cell suspension was recovered and centrifuged at 400 g for 5 min, then resuspended in DMEM with 20% fetal bovine serum (FBS, HyClone), 2% penicillin–streptomycin, and cultured in plates. The cells used in the experiments were from passages 3 to 5.

Animals

Six-week-old male C57BL/6 mice and ApoE$^{-/-}$ mice were purchased from Beijing Hfk Bioscience. All mice were maintained in a temperature- and light-controlled facility, and permitted *ad libitum* consumption of water. These mice were fed either a standard control diet (SCD) or western diet (WD) for 16 weeks. ApoE$^{-/-}$ mice were intravenously administrated with adenovirus (Ad-SM22-EV or Ad-SM22-Nron; n = 12 per group) every two weeks in the last 8 weeks before sacrificed, or received a single intravenous injection of adeno-associated virus 2/8 (rAAV-shNC or rAAV-shNron; n = 12 per group) after WD feeding for 4 weeks. All procedures involving animals and animal care protocols conformed to the Guideline for the Care and Use of Laboratory Animals published by the US National Institutes of Health (NIH), and were approved by the Ethics Committee of Union Hospital, Huazhong University of Science and Technology, China.

Human atherosclerotic tissues

Eight human atherosclerotic lesions were collected from patients undergoing carotid endarterectomy at Wuhan Union Hospital. 10 internal mammary arteries obtained from patients undergoing coronary artery

bypass surgery were used as non-atherosclerotic control arteries. Written informed consent was obtained from all participants according to the Declaration of Helsinki.

METHOD DETAILS

Generation of recombinant adenovirus and adeno-associated virus

Adenovirus carrying control GFP (Ad-SM22-EV) or Nron cDNA driven by the SM22α promoter (Ad-SM22-Nron) was employed to induce overexpression (OE) of Nron in VSMC of ApoE$^{-/-}$ mice. Recombinant adeno-associated virus 2/8 [rAAV 2/8, AAV2 inverted terminal repeats (ITR) DNA combined with the AAV serotype 8 capsid] carrying scramble shRNA or Nron shRNA was employed to knock down the expression of Nron in ApoE$^{-/-}$ mice. All recombinant adenovirus and AAV were provided by Shanghai GeneChem.

Histological analysis and quantification of atherosclerotic lesions

Mice were fasted for 4 h and then anesthetized. Lipid accumulation of thoracoabdominal aorta was determined by *en face* Oil Red O staining. Briefly, mouse aortas were dissected longitudinally with an extremely fine Vanna microscissor and pinned flat on a black wax surface with 0.2-mm-diameter stainless steel pins. The pinned aortas were stained with Oil Red O and images were captured with a standard digital camera. For the microscopic evaluation of the aortic sinus lesions, hearts were fixed in 4% paraformaldehyde and cryopreserved in 15% sucrose, and then 30% sucrose. After embedded in OCT compound (Sakura Finetek, Torrance, CA), hearts were cryosectioned and 6-μm sections were collected at 80-μm intervals, starting at a 100-μm distance from the appearance of the aortic valves. Aortic sinus sections were stained with Oil red O for lipid accumulation, with hematoxylin and eosin (HE) for morphology, with Masson's trichrome staining (Masson) for collagen content, with elastica van Gieson staining (EVG) for elasticfibers. The relative content of macrophages and smooth muscle cells were detected by immunohistochemistry. Frozen serial sections were treated with 0.3% H_2O_2 in PBS to block endogenous peroxidase activity, followed by blocking in 4% BSA (Sigma). Primary antibodies specific for F4/80 (ab100790, Abcam), α-SMA (ab240654, Abcam) or VEGFA (ab1316, Abcam) was used. All sections were stained with biotinylated secondary antibodies and detected using ABC reagents (K-850275, Vector Laboratories). Images were captured by optical microscope and quantitated by quantitative morphometry with Image Pro Plus. The lesion areas were determined by calculating the mean lesion area of the four sections at 80-μm intervals. To evaluate the relative content of the stained constituents, the percentage of blue (collagen on Masson's trichrome staining) and DAB-positive (immunohistochemistry) areas to the total plaque areas was determined. Fibrous cap area was quantified as a percent of total plaque area. We defined fibrous caps as the VSMC and proteoglycan-rich area overlying the cholesterol-rich, matrix-poor, acellular regions of the necrotic cores (Clarke et al., 2006). Elastic lamina destruction of the tunica media was evaluated by quantifying the ruptures (i.e. discontinuities or fractures) of elastic fibers (de Nooijer et al., 2009). To detect intimal capillaries, the aortic sinus sections with substantial lesions were incubated with anti-CD31 antibody (ab182981, Abcam). Positive staining of the endothelium on the lumen and in adventitial capillaries served as an internal control. Intimal vessels were identified under high power (×400) and counted when both an endothelial cell nucleus and lumen were seen and when the vessel was also observed in an adjacent section.

RNA fluorescence *in situ* hybridization

The *in situ* detection of Nron was performed on 6-μm formalin fixed, paraffin-embedded sections using miRCURY LNA^{TM} detection probe (LNA-modified and DIG-labeled oligonucleotide; Exiqon). The probe sequence of Nron is listed as follows: 5′–3′/5DigN/TAAAGGAGCAGTGGTAGAAACA/3DigN/. RNA FISH assay was performed following a protocol adapted from the manufacturer's instruction. Briefly, the slides were hybridized with the probe complementary to Nron, followed by incubation with anti-DIG FITC-conjugated Fab fragments. Scrambled control RNA was included for each hybridization procedure. Subsequently, sections were immersed with mounting medium (ProLong Gold anti-fade reagent with DAPI, Invitrogen) to stain nuclei and subjected to fluorescent signal detection.

Immunofluorescence

Immunofluorescence on human carotid artery sections and mice aortic sinus sections was performed. Briefly, for double-staining, sections were incubated with anti-α-SMA antibody (ab240654, Abcam), together with anti-NFATc1 antibody (ab25916, Abcam), anti-NFATc2 antibody (sc-7296, Santa Cruz), anti-NFATc3 antibody (sc-8405, Santa Cruz) or anti-NFATc4 antibody (ab99431, Abcam) at 4°C overnight, followed by a 30-min incubation with secondary antibody conjugated to Alexa Fluor 594 (R37121, Molecular

probes) and Alexa Fluor 488 (R37116, Molecular probes). The signals of individual and merged images for antigen detection were performed using a fluorescence microscope (Olympus, Japan) and Axiovision 4.8 software.

RNA extraction and qRT-PCR

Total RNA was extracted from cells or tissues with the use of TRIzol reagent (D9108A, Takara Bio). RNA was reverse-transcribed using the PrimeScript™ RT Master Mix (RR036A, Takara Bio). cDNA samples were analyzed by quantitative polymerase chain reaction (qPCR) using One Step SYBR PrimeScript™ RT-PCR Kit (RR066A, Takara Bio). DNA amplification was performed with an ABI PRISM 7900 Sequence Detector system (Applied Biosystem, Foster City, CA), following the manufacturer's instructions. Relative gene expression (normalized to endogenous control gene β-actin) was calculated using the comparative Ct method. Primer sequences are provided in Table S3.

Western blot

Cells were harvested at the indicated time points and homogenized in ice-cold suspension buffer supplemented with a proteinase inhibitor cocktail (P8340, Sigma). Protein concentrations were determined using the BCA Protein assay kit (A53226, Thermo Scientific). Equal amounts of protein were fractionated by SDS polyacrylamide gels, followed by immunoblotting with anti-NFATc3 antibody (sc-8405, Santa Cruz) or anti-VEGFA antibody (ab1316, Abcam). Membranes were then incubated with peroxidase-conjugated secondary antibody, and specific bands were detected with a Bio-Rad imaging system (Hercules, CA).

RNA pull-down and mass spectrometry

The biotin-labeled full-length Nron and antisense Nron were synthesized using the Biotin RNA Labeling Mix and T7 RNA polymerase (18033019, Invitrogen), and purified with the RNeasy Mini Kit (74106, QIAGEN) on-column digestion of DNA. RNA pull-down assays were performed with the Pierce™ magnetic RNA–protein pull-down kit (20164, Thermo Fisher Scientific) according to the manufacturer's instructions. Briefly, the proteins exacted from mouse primary VSMCs were respectively incubated with the biotin-labeled sense and anti-sense RNA at room temperature for 4 h, followed by the incubation with streptavidin beads at 4°C overnight. After that, the unbounded proteins were removed, while the bounded proteins were eluted and further analyzed by electrophoresis and silver-staining (Pierce silver stain kit, 24612, Thermo Scientific). For Mass Spectrometry, a specific band present in the sense RNA lane was extracted (corresponding region in the anti-sense RNA lane was also extracted as control) for further analysis.

RNA immunoprecipitation

Cells were treated with 0.3% formaldehyde for 10 min at 37°C. 1.25 M glycine dissolved in PBS was added to a concentration of 0.125 M, and the sample was incubated for 5 min at room temperature. Then cells were washed twice in PBS and pelleted. The pellet was resuspended in RIPA buffer (50 mM Tris, pH 7.4, 150 mM NaCl, 1 mM EDTA, 0.1% SDS, 1% NP-40, 0.5% sodium deoxycholate, 0.5 mM DTT and 1 mM PMSF/cocktail), incubated on ice with frequent vortex for 30 min NFATc3 antibody or IgG were added and samples were incubated overnight at 4°C. The RNA/protein complex was recovered with protein G Dynabeads and washed with RIPA buffer several times. RNA was recovered with Trizol and analysed by RT–PCR.

VSMC proliferation assay

Proliferation of VSMCs was assessed by EdU (5-ethynyl-20-deoxyuridine) assay using Cell-Light EdU Apollo 567 *In Vitro* Kit (C10310, RiboBio, Guangzhou, China). VSMCs were seeded in six-well plates overnight. After the indicated treatment, the culture medium was replaced with DMEM containing 50 μM EdU and incubated for another 2 h. The cells were fixed in PBS containing 4% paraformaldehyde for 30 min and stained according to the manufacturer's instructions. The numbers of EdU-positive cells were counted in five randomly chosen fields (magnification, ×200).

VSMC migration assay

With the modified Boyden chamber method, SMC migration is determined in Transwell cell culture chambers with 8 mm pores (Millipore, Billerica, MA, USA). VSMCs (5×10^4 cells per well) suspended in 100 μ of DMEM was added to the upper chamber. Migration was induced by the addition of 10% FBS in DMEM to the lower compartment. After 5 h of incubation, cells on both side of the membrane were fixed and stained with 1% toluidine blue (Sigma-Aldrich). Cells on the upper side of the membrane were removed

with a cotton swab. The average number of cells from five randomly chosen high power (200X) fields on the lower side of the membrane was counted.

VSMC Tunel assay

The Tunel assay was performed with the One-Step TUNEL Apoptosis Kit (C11026, RiboBio, Guangzhou, China). VSMCs were cultured on glass coverslips in a 12-well plate at a density of 2×10^5 cells/well. After ox-LDL and siRNA treatment, VSMCs were washed with PBS and fixed in 4% paraformaldehyde for 10 min at room temperature. The fixed cells were then incubated for 2 min on ice in a permeabilization solution (0.1% Triton X-100 in 0.1% sodium citrate). The slides were rinsed with PBS before the rTdT incubation mixture was added. After incubation for 60 min at 37°C, the slides were rinsed three times with 2× SSC, and the nuclei were counterstained with DAPI. The numbers of Tunel-positive cells were counted in five randomly chosen fields (magnification, ×200).

Tube formation assay

Mouse aortic endothelial cells (MAECs) were seeded at 4×10^4/well in 96-well plates coated with ECMatrix (BD Bioscience). Then cells were treated with medium from Nron OE VSMCs alone or with combined VEGFR2 siRNA. The total tube length and branch points were calculated and analyzed using the "Angio-genesis Analyzer" tool of Image J software (Gupta et al., 2004).

QUANTIFICATION AND STATISTICAL ANALYSIS

GraphPad Prism software (GraphPad Software Inc., La Jolla, CA) was used for statistical analyses. Band intensity in western blot images was quantified with Image J Software. Values are expressed as means ± SEM of at least three independent experiments. Student's t test was used to assess the statistical significance of the differences between two groups. For multiple groups, significance was evaluated by one-way ANOVA with Bonferroni test (homogeneity of variance) or Tamhanes's T2 test (heterogeneity of variance). $p < 0.05$ was considered statistically significant. Randomization and blinding strategy was used whenever possible. Animal cohort sizes were determined on the basis of similar previous studies.